Draft version September 3, 2026
Typeset using LaTeX twocolumn style in AASTeX7.0.1

Cross-scale CO-to-H_2 Conversion Factor Prescriptions Based on CO Line Properties

Yu-Hsuan Teng [1], Alberto D. Bolatto [1,2], Jiayi Sun [3], I-Da Chiang [4], Karin M. Sandstrom [5], Adam K. Leroy [6], Jakob den Brok [7], Antonio Usero [8], Jonathan D. Henshaw [7], Oscar Agertz [9], Amirnezam Amiri [10,11], Dario Colombo [12], Simon C. O. Glover [13], Ralf S. Klessen [13,14], Hsi-An Pan [15], Vicente Villanueva [16,17] and Thomas G. Williams [18]

[1] *Department of Astronomy, University of Maryland, 4296 Stadium Drive, College Park, MD 20742, USA*
[2] *Joint Space-Science Institute, University of Maryland, College Park, MD 20742, USA*
[3] *Department of Physics and Astronomy, University of Kentucky, 506 Library Drive, Lexington, KY 40506, USA*
[4] *Center of Astronomy and Gravitation, National Taiwan Normal University, No. 88, Sec. 4, Ting-Chou Rd., Taipei 116, Taiwan*
[5] *Department of Astronomy & Astrophysics, University of California San Diego, 9500 Gilman Drive, La Jolla, CA 92093, USA*
[6] *Department of Astronomy, The Ohio State University, 140 West 18th Avenue, Columbus, OH 43210, USA*
[7] *Max-Planck-Institut für Astronomie, Königstuhl 17, D-69117, Heidelberg, Germany*
[8] *Observatorio Astronómico Nacional (IGN), C/Alfonso XII, 3, E-28014 Madrid, Spain*
[9] *Lund Observatory, Division of Astrophysics, Department of Physics, Lund University, Box 118, SE-221 00 Lund, Sweden*
[10] *School of Astronomy, Institute for Research in Fundamental Sciences (IPM), Tehran, P.O. Box 19395-5531, Iran*
[11] *Department of Physics, University of Arkansas, 226 Physics Building, 825 West Dickson Street, Fayetteville, AR 72701, USA*
[12] *Argelander-Institut für Astronomie, Universität Bonn, Auf dem Hügel 71, 53121 Bonn, Germany*
[13] *Universität Heidelberg, Zentrum für Astronomie, Institut für Theoretische Astrophysik, Albert-Ueberle-Str. 2, 69120 Heidelberg, Germany*
[14] *Universität Heidelberg, Interdisziplinäres Zentrum für Wissenschaftliches Rechnen, Im Neuenheimer Feld 225, 69120 Heidelberg, Germany*
[15] *Department of Physics, Tamkang University, No.151, Yingzhuan Road, Tamsui District, New Taipei City 251301, Taiwan*
[16] *Instituto de Estudios Astrofísicos, Facultad de Ingeniería y Ciencias, Universidad Diego Portales, Av. Ejército Libertador 441, 8370191 Santiago, Chile*
[17] *Millennium Nucleus for Galaxies, MINGAL*
[18] *UK ALMA Regional Centre Node, Jodrell Bank Centre for Astrophysics, Department of Physics and Astronomy, The University of Manchester, Oxford Road, Manchester M13 9PL, UK*

ABSTRACT

Accurate measurements of molecular gas mass in galaxies rely on the CO-to-H_2 conversion factor ($\alpha_{\rm CO}$), which is known to vary with galactic environments. While recent studies have shown that CO velocity dispersion and ^{12}CO/^{13}CO line ratios ($R_{12/13}$) reliably trace $\alpha_{\rm CO}$ variation on ∼100-pc scales, whether these prescriptions extend to lower-resolution observations or broader galactic environments remains unexplored. Using recent dust-based, kpc-scale $\alpha_{\rm CO}$ measurements and CO observations from PHANGS-ALMA, we investigate the dependence of $\alpha_{\rm CO}$ on inclination-corrected local CO velocity dispersion (Δv) across varying spatial resolutions from 250 pc up to 2 kpc, in a sample of 12 nearby galaxies. We find that the $\alpha_{\rm CO}$-Δv anti-correlation holds up to 2-kpc scales with a ±0.2 dex scatter, showing consistent power-law slopes ranging from 0.74–0.96 and increasing intercepts with increasing spatial scales. These cross-scale $\alpha_{\rm CO}$-Δv relations can be explained by the strong correlations between Δv measured from both 150-pc and up to 2-kpc scales, which is due to major contributions from internal cloud dynamics (as inferred from the 150-pc beam size) on kpc-scale Δv measurements. We also explore $R_{12/13}$ as a potential cross-scale $\alpha_{\rm CO}$ indicator across 7 nearby galaxies, noting a decreasing $\alpha_{\rm CO}$-$R_{12/13}$ trend at 1.5-kpc resolution that aligns with previous barred galaxy results at ∼100 pc. Overall, these robust, cross-scale $\alpha_{\rm CO}$ prescriptions based on CO line properties provide a practical tool for CO-based galaxy studies across a wide range of spatial scales, enabling accurate $\alpha_{\rm CO}$ derivations especially in environments where conventional $\alpha_{\rm CO}$ treatments may be insufficient.

Corresponding author: Yu-Hsuan Teng
Email: yhteng@umd.edu

Keywords: CO line emission (262) — Disk galaxies (391) — Galaxy dynamics (591) — Giant molecular clouds (653) — Star formation (1569)

1. INTRODUCTION

Assessing the amount of molecular hydrogen (H_2) in galaxies is fundamental to understanding star formation, a process governed by the conversion of molecular gas into stars (C. F. McKee & E. C. Ostriker 2007; M. R. Krumholz 2014; R. S. Klessen & S. C. O. Glover 2016; P. Girichidis et al. 2020). To trace the bulk distribution of molecular gas in galaxies, astronomers often measure low-J rotational lines of carbon monoxide (CO) and assume a CO-to-H_2 conversion factor ($\alpha_{\rm CO}$; review by A. D. Bolatto et al. 2013). However, $\alpha_{\rm CO}$ is not a universal constant, and it is known to vary significantly with local environmental conditions (e.g., $\alpha_{\rm CO}$ in starbursts or metal-poor environments can vary by 1–2 orders of magnitude; D. Narayanan et al. 2012; P. P. Papadopoulos et al. 2012; K. M. Sandstrom et al. 2013; F. Renaud et al. 2019; M. Gong et al. 2020). For decades, this variation of $\alpha_{\rm CO}$ has therefore introduced major systematic uncertainties into the measurements of star formation properties, such as molecular cloud free-fall time, virial parameter, and star formation efficiency (e.g., J. Sun et al. 2022, 2023; Y.-H. Teng et al. 2024).

Theoretical studies suggested that CO opacity (or optical depth, equivalently) is a key physical driver of $\alpha_{\rm CO}$ variations in star-forming galaxies, particularly in starburst environments (R. Shetty et al. 2011; D. Narayanan et al. 2012; P. P. Papadopoulos et al. 2012). Recent observational studies further confirmed a strong correlation between the measured $\alpha_{\rm CO}$ and CO opacity (Y.-H. Teng et al. 2022, 2023; H. He et al. 2024), using multi-line CO isotopologue modeling at the ~100-pc scale of giant molecular clouds (GMCs). As low-J ^{12}CO lines remain optically thick in most nearby galaxy observations, a lower CO opacity can decrease the $\alpha_{\rm CO}$ value due to an increased CO emissivity. For instance, a broadened CO line width can lead to a lower opacity that explains why $\alpha_{\rm CO}$ is low in galaxy centers (e.g., A. D. Bolatto et al. 2013; Y.-H. Teng et al. 2022). Furthermore, the ^{12}CO/^{13}CO line ratios may also trace CO opacity, since ^{12}CO is mostly optically thick ($\tau \gg 1$) while ^{13}CO is optically thinner (with $\tau < 1$ in molecular clouds; e.g., J. E. Pineda et al. 2008; L. Szűcs et al. 2014). Therefore, the strong $\alpha_{\rm CO}$ dependence on CO opacity has further inspired $\alpha_{\rm CO}$ prescriptions based on CO velocity dispersion (Y.-H. Teng et al. 2024) and potentially the ^{12}CO/^{13}CO line ratios (T. A. D. Paglione et al. 2001; D. Cormier et al. 2018; Y.-H. Teng et al. 2023; H. He et al. 2024; J. den Brok et al. 2025a).

While these CO-based $\alpha_{\rm CO}$ prescriptions represent a significant step forward, they are primarily developed and verified on ~100-pc scales, which are currently difficult to reach and thus have limited their applicability. However, how much these prescriptions can be extended to coarser angular-resolution observations remains unexplored. It is likely that these prescriptions are valid up to certain scales, given that the large variability of CO line properties and $\alpha_{\rm CO}$ on small spatial scales may average out (e.g., M. Kohno & Y. Sofue 2024), or trace non-GMC-associated properties such as galactic rotation or cloud-to-cloud motions that should not impact $\alpha_{\rm CO}$. As extragalactic surveys increasingly provide molecular gas measurements across large galaxy samples at different scales (e.g., A. D. Bolatto et al. 2017; G. Calistro Rivera et al. 2018; K. Sorai et al. 2019; L. Lin et al. 2020; A. K. Leroy et al. 2021a; F. Rizzo et al. 2023), it is important to understand how $\alpha_{\rm CO}$ prescriptions perform when averaged over larger physical scales.

Motivated by the recent development in CO-based $\alpha_{\rm CO}$ prescriptions on ~100-pc scales, this paper tests and expands those prescriptions across varying resolutions from 250-pc up to 2-kpc scales. Our primary goal is to uncover the physical meanings behind these prescriptions and optimize their applicability for galaxy studies across different observational resolutions.

2. DATA AND MEASUREMENTS

2.1. *Dust-based $\alpha_{\rm CO}$ Measurements*

We obtain dust-based $\alpha_{\rm CO}$ measurements from I.-D. Chiang et al. (2024), where $\alpha_{\rm CO}$ is derived by assuming a metallicity-dependent dust-to-gas ratio over 2-kpc-sized hexagonal apertures. This provides a $\alpha_{\rm CO}$ grid sampled on ~500-pc scales (but represents 2-kpc-scale $\alpha_{\rm CO}$) across galaxies. We adopt these gridded measurements to investigate $\alpha_{\rm CO}$ correlations with CO line properties at varying resolutions, aiming to expand $\alpha_{\rm CO}$ prescriptions to various observational scales.

Our main results focus on the same 12 nearby galaxies as in Y.-H. Teng et al. (2024), which are the intersection between I.-D. Chiang et al. (2024) and the PHANGS-ALMA samples (A. K. Leroy et al. 2021a). The $\alpha_{\rm CO}$ of these galaxies were inferred directly from the PHANGS CO (2–1) data, and we use the version with a constant CO (2–1)/(1–0) ratio of 0.65 (Y. Yajima et al. 2021; A. K. Leroy et al. 2022; J. den Brok et al. 2025b) for consistency with Y.-H. Teng et al. (2024) and to facilitate reproducibility. We also adopt the $\alpha_{\rm CO}$ of 7 galaxies overlapping with the CO Multi-line Imaging of Nearby Galaxies (COMING; K. Sorai et al. 2019) sample, where $\alpha_{\rm CO}$ was also directly derived from the COMING CO (1–0) data in I.-D. Chiang et al. (2024).

2.2. *Multi-scale PHANGS Datasets*

We generate CO (2–1) map products convolved to 250-pc, 500-pc, 750-pc, 1-kpc, 1.5-kpc, and 2-kpc scales using the PHANGS-ALMA pipeline (A. K. Leroy et al. 2021b) for all 12 PHANGS galaxies (see A. K. Leroy et al. 2021a; Y.-H. Teng et al. 2024, for basic galaxy properties). The best common resolution data at 150-pc or 90-pc scales, including cubes and kpc-averaged statistics (from J. Sun et al. 2022) are also used for comparison purposes. Specifically, we use the pipeline-produced 'strict' maps of moment-1 and effective line width[19] to analyze gas dynamical properties and scaling relations at different scales. As our explored data resolutions are either similar or lower than the $\alpha_{\rm CO}$ grid sampling rate (§2.1), we simply adopt nearest-neighbor matching based on the $\alpha_{\rm CO}$ grid when connecting $\alpha_{\rm CO}$ with CO observations (§3.1).

2.3. *COMING CO and* ^{13}*CO Datasets*

We investigate the kpc-scale relationship between $\alpha_{\rm CO}$ and ^{12}CO/^{13}CO line ratios ($R_{12/13}$) in §3.3, using data products for ^{12}CO (1–0) and ^{13}CO (1–0) from the COMING survey (K. Sorai et al. 2019, based on 17″ ($\sim$kpc) observations from the Nobeyama Radio Observatory 45-m telescope), which is publicly available on the Nobeyama FITS Data Archive[20]. While the COMING survey targeted ^{12}CO, some galaxies were also detected in ^{13}CO, and seven of these galaxies have spatially resolved $\alpha_{\rm CO}$ measurements from I.-D. Chiang et al. (2024) directly derived for CO (1–0).

3. RESULTS

3.1. $\alpha_{\rm CO}$ *Dependence on* CO *Velocity Dispersion*

To investigate whether $\alpha_{\rm CO}$ variations with Δv can extend to physical scales beyond 150 pc (Y.-H. Teng et al. 2024), we evaluate the varying-resolution Δv maps on the positions of the $\alpha_{\rm CO}$ sampling grid (§2.2). Figure 1 presents the $\alpha_{\rm CO}$-Δv relations, with Δv evolving from 250-pc to 2-kpc resolutions[21]. The gray areas show the low-confidence regime where $\alpha_{\rm CO}$ sampling is incomplete (i.e., the fraction of reliable $\alpha_{\rm CO}$ data per velocity bin is below 50%; see Y.-H. Teng et al. 2024). In addition, all the Δv values have been corrected for galaxy inclination by a factor of $\sqrt{\cos(i)}$ (following Y.-H. Teng et al. 2024), which is an empirical correction derived in J. Sun et al. (2022, Appendix C) to eliminate the inclination dependency of observed Δv.

After excluding the data-incomplete regime (i.e., gray shaded areas in Figure 1), we conduct a least-squares fitting in log-log space:

$$\log \alpha_{\rm CO} = m \ \log \Delta v_i + b \ , \tag{1}$$

where i indicates the resolution scale of Δv, and the best-fit m and b are listed in Table 1 as well as annotated on the figure panels. For data from 250-pc to 2-kpc scales, the dispersion with respect to Equation 1 is constantly below 0.2 dex, and the Pearson correlation coefficients are 0.6–0.7 with p-values $\ll 0.05$.

As shown in Figure 1, all resolution scales result in a clear anti-correlation between $\alpha_{\rm CO}$ and Δv. The best-fit slopes (dotted lines) are generally at $\sim$0.8 (ranging from $\sim$0.7–1.0), which agree well with the relation in Y.-H. Teng et al. (2024) based on $\Delta v_{\rm 150pc}$ (dashed lines). The slight drift of the slopes and clear increase of the intercept b with increasing scales mainly reflects the rise of Δv due to larger-scale motions being included within larger beam sizes. We also note that NGC 4536 and 4569 are barred galaxies with centers showing the brightest kpc-averaged CO intensity across our sample (Y.-H. Teng et al. 2024, Table 1), and thus bar-driven inflows and increased emissivity in their centers may explain the substantial $\alpha_{\rm CO}$ drop at high Δv.

Table 1 lists our best-fit coefficients and errors for the $\alpha_{\rm CO}$-Δv relations from 250-pc to 2-kpc scales. Overall, the consistent $\alpha_{\rm CO}$-Δv trends and slopes seen across varying scales suggest that Δv can be a good $\alpha_{\rm CO}$ indicator, not only at near-GMC scale but also extended up to kpc scales. Thus, the reported functional fits may be broadly used to estimate the varying $\alpha_{\rm CO}$ values for CO observations across nearby galaxies. In the latest CO (1–0) observations from the Extragalactic Database for Galaxy Evolution (EDGE) surveys (Y.-H. Teng et al. 2026), our 2-kpc-scale prescription was already adopted and compared to existing prescriptions systematically.

3.2. *Why Does Large-scale* Δv *Work to Trace* $\alpha_{\rm CO}$*?*

3.2.1. *Tracking 150-pc* Δv *with kpc-scale* Δv

The original $\alpha_{\rm CO}$-Δv prescription in Y.-H. Teng et al. (2024) was based on the average of intensity-weighted effective line widths measured at 150-pc scales over separate 1.5-kpc-sized hexagonal regions ($\langle \Delta v \rangle_{\rm 150pc}$; see J. Sun et al. 2022). To connect with the original prescription, we obtain the same $\langle \Delta v \rangle_{\rm 150pc}$ values and compare

[19] Defined as $I_{\rm CO}/(\sqrt{2\pi}\, T_{\rm peak})$, which is identical to moment-2 for a Gaussian line profile (A. K. Leroy et al. 2021b).

[20] https://jvo.nao.ac.jp/portal/nobeyama/coming.do

[21] We do not extend beyond 2 kpc because it is the resolution of our dust $\alpha_{\rm CO}$ measurements.

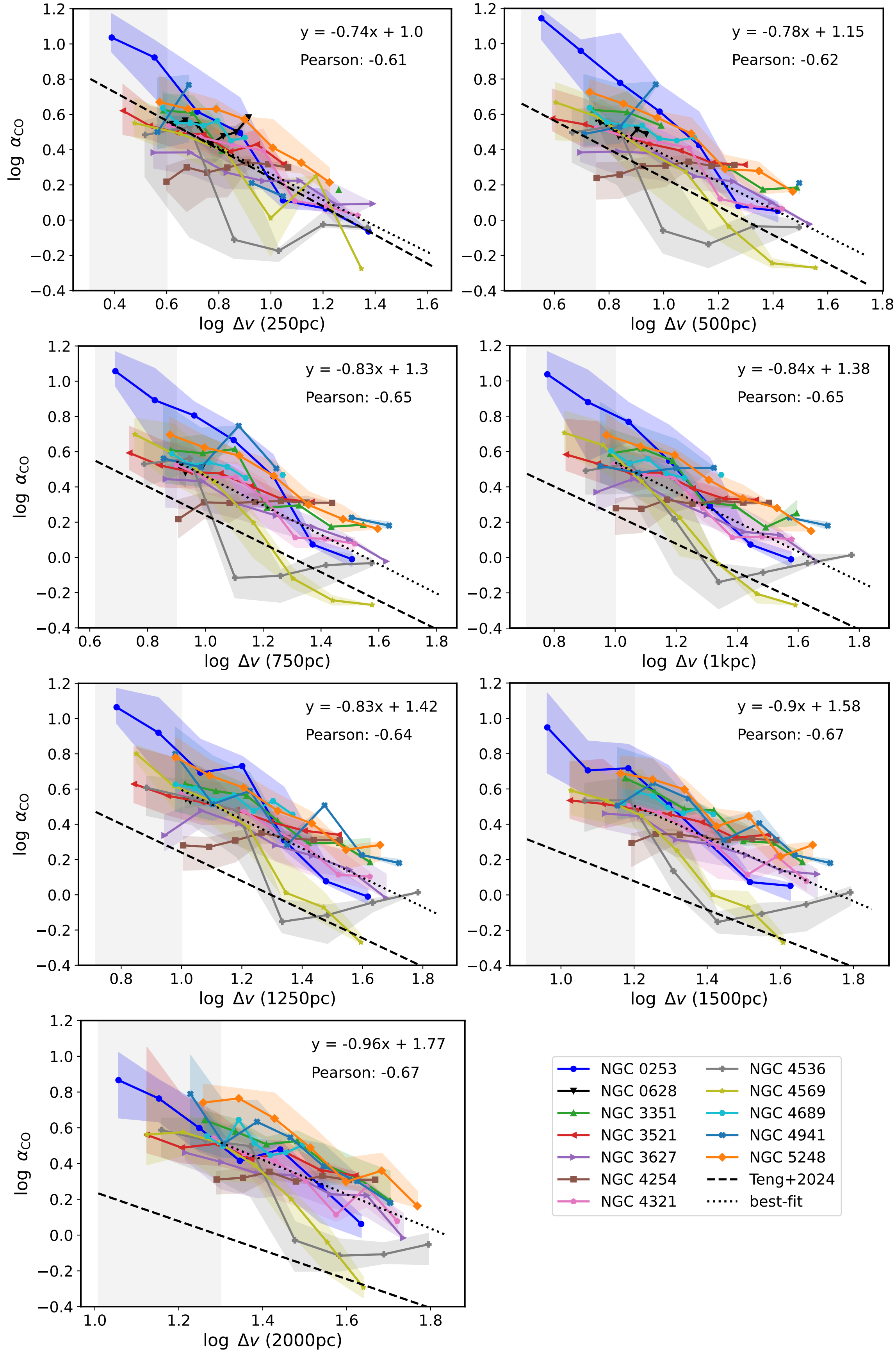

Figure 1. All 12 galaxies show clear anti-correlations between $\alpha_{\rm CO}$ ($M_\odot$ (K km s^{-1})$^{-1}$ pc^{-2}) measured at 2-kpc scales and CO velocity dispersion (km s^{-1}) from 250-pc to 2-kpc resolutions, suggesting that Δv can be a good $\alpha_{\rm CO}$ indicator for CO observations in a wide range of scales. The colored lines and shaded areas represent the binned medians and $\pm 1\sigma$ range for each galaxy, respectively. The dotted line shows the best-fit power law relation, excluding the low-Δv regimes with incomplete data sampling (shaded in gray). The dashed line shows the relation from Y.-H. Teng et al. (2024) based on Δv at 150-pc scales.

Table 1. Best-fit Power Law Coefficients

Resolution	m	b
	$\log \alpha_{\rm CO} = m \log(\Delta v) + b$	
*90 pc	-0.59 ± 0.04	0.90 ± 0.03
*150 pc	-0.81 ± 0.02	1.05 ± 0.02
250 pc	-0.74 ± 0.03	1.00 ± 0.02
500 pc	-0.78 ± 0.03	1.15 ± 0.02
750 pc	-0.83 ± 0.03	1.30 ± 0.03
1 kpc	-0.84 ± 0.03	1.38 ± 0.03
1.25 kpc	-0.83 ± 0.03	1.42 ± 0.03
1.5 kpc	-0.90 ± 0.03	1.58 ± 0.04
2 kpc	-0.96 ± 0.04	1.77 ± 0.05
	$\log\langle\Delta v\rangle_{\rm 150pc} = m \log(\Delta v) + b$	
1.25 kpc	0.76 ± 0.03	-0.14 ± 0.03
1.5 kpc	0.74 ± 0.03	-0.16 ± 0.03
2 kpc	0.68 ± 0.03	-0.16 ± 0.03

NOTE—* The best-fit $\alpha_{\rm CO}$-Δv relations for 90-pc and 150-pc resolutions (based on the same 12 galaxies) are from Y.-H. Teng et al. (2024, Figure 1a). The functional form of the 90-pc relation was not explicitly listed in that paper but has been used and reported in subsequent studies (e.g., M. Sánchez-García et al. 2026).

them with our varying-resolution Δv maps (§2.2). As $\langle\Delta v\rangle_{\rm 150pc}$ is an averaged quantity over 1.5-kpc apertures, we only compare with maps at similar (1.25–2-kpc) scales to avoid biases from cross-scale matching.

Figure 2 shows that $\langle\Delta v\rangle_{\rm 150pc}$ correlates well with Δv measured from 1.25-kpc to 2-kpc scales, with only a $\sigma \sim 0.1$ dex scatter. These correlations among cross-scale Δv indicate that $\langle\Delta v\rangle_{\rm 150pc}$ can be well-tracked by lower-resolution Δv even up to 2-kpc. The dotted lines show the best-fit Δv relations across scales (see also Table 1). The Pearson correlation coefficient (best-fit slope) decreases from 0.71 (0.76) at 1.25-kpc to 0.58 (0.68) at 2-kpc. While the scatter increases with scales, the positive correlations between $\langle\Delta v\rangle_{\rm 150pc}$ and Δv are still significant on 2-kpc scales.

The finding that $\langle\Delta v\rangle_{\rm 150pc}$ correlates well with Δv up to 2-kpc scale explains why the anti-correlation between $\alpha_{\rm CO}$ and Δv also extends up to kpc scales (§3.1 and Figure 1). In other words, while the $\alpha_{\rm CO}$-Δv relation is found to be the strongest at near-GMC resolutions (with a dispersion $\sigma \sim 0.1$ dex at 150-pc scale; Y.-H. Teng et al. 2024), the correlations between 150-pc and larger-scale Δv further lead to similar $\alpha_{\rm CO}$-Δv trends up to 2-kpc scales, albeit with an increased scatter of $\sigma \lesssim 0.2$ dex. This implies that our kpc-scale $\alpha_{\rm CO}$ prescriptions (upper part of Table 1) is similar to deriving $\langle\Delta v\rangle_{\rm 150pc}$ via the Δv relations (lower part of Table 1) and then substituting it into the original prescription in Y.-H. Teng et al. (2024). However, such indirect computing process may induce additional $\alpha_{\rm CO}$ uncertainty ($\sim$0.3 dex) propagated from the scatter in both relations, and thus we recommend using the direct $\alpha_{\rm CO}$-Δv relations whenever possible.

In Figure 2, the overall distribution of Δv also shifts with scales, deviating increasingly from the 1-to-1 relation (dashed lines). This may indicate a diminishing contribution of GMC-scale motions over larger scales (more in §3.2.2). The Δv offset in the bottom panel ($\sim$0.5 dex between 150-pc and 2-kpc) is also roughly consistent with the Kolmogorov-like scaling in size-linewidth relations (R. B. Larson 1981; B. G. Elmegreen & Y. N. Efremov 1996), which may support a scenario of turbulence cascade up to kpc scales (more in §4.1).

3.2.2. *Contribution from 150 pc-scale Δv in kpc apertures*

The strong correlations between multi-scale Δv (Figure 2) suggest that Δv measured at near-GMC (150-pc) scale makes a key contribution on kpc scales. To quantify this we define kpc-size apertures over the central 5 kpc of our galaxies, and in each of them we stack the 150-pc scale spectra centering on the velocity from the 150-pc moment-1 map (A. Schruba et al. 2011, see also Y.-H. Teng et al. 2022), thus obtaining a representative 150-pc scale velocity dispersion for each aperture. Figure 3 illustrates this process. The top panels of 3b and 3c show the results of this procedure for the center and for a representative position in the disk. The bottom panels demonstrate that the effects of beam-smearing on kpc-scale spectra are large in the center, but much less dominant in the disk where $\Delta v_{\rm 150pc} \sim 5$ km s^{-1} and $\Delta v_{\rm kpc} \sim 10$ km s^{-1} only differ by a factor of 2.

We find that the below-factor-of-2 increase in Δv from 150-pc to 1-kpc scales is a general case across galaxy disks (see Appendix A for statistics of $\Delta v_{\rm 150pc}$ and $\Delta v_{\rm kpc}$ over all central and disk apertures). This suggests that molecular cloud dynamics within 150-pc scales does contribute to a good fraction[22] of kpc-scale line widths, such that $\Delta v_{\rm kpc}$ still correlates with $\Delta v_{\rm 150pc}$ (§3.2.1), thereby leading to the extension of $\alpha_{\rm CO}$-Δv anti-correlations up to kpc scales (§3.1).

To check if our $\Delta v_{\rm 150pc}$ derived from spectral stacking and Gaussian fitting effectively represent gas dynamics on 150-pc scales, we relate the measured $\alpha_{\rm CO}$ with our fitted line widths from stacking ($\Delta v_{\rm fit}$) in Figure 4a, which reveals a strong anti-correlation consistent with the Y.-H. Teng et al. (2024) prescription. This agree-

[22] But not necessarily a dominant fraction, if Δv contributions add up in quadrature.

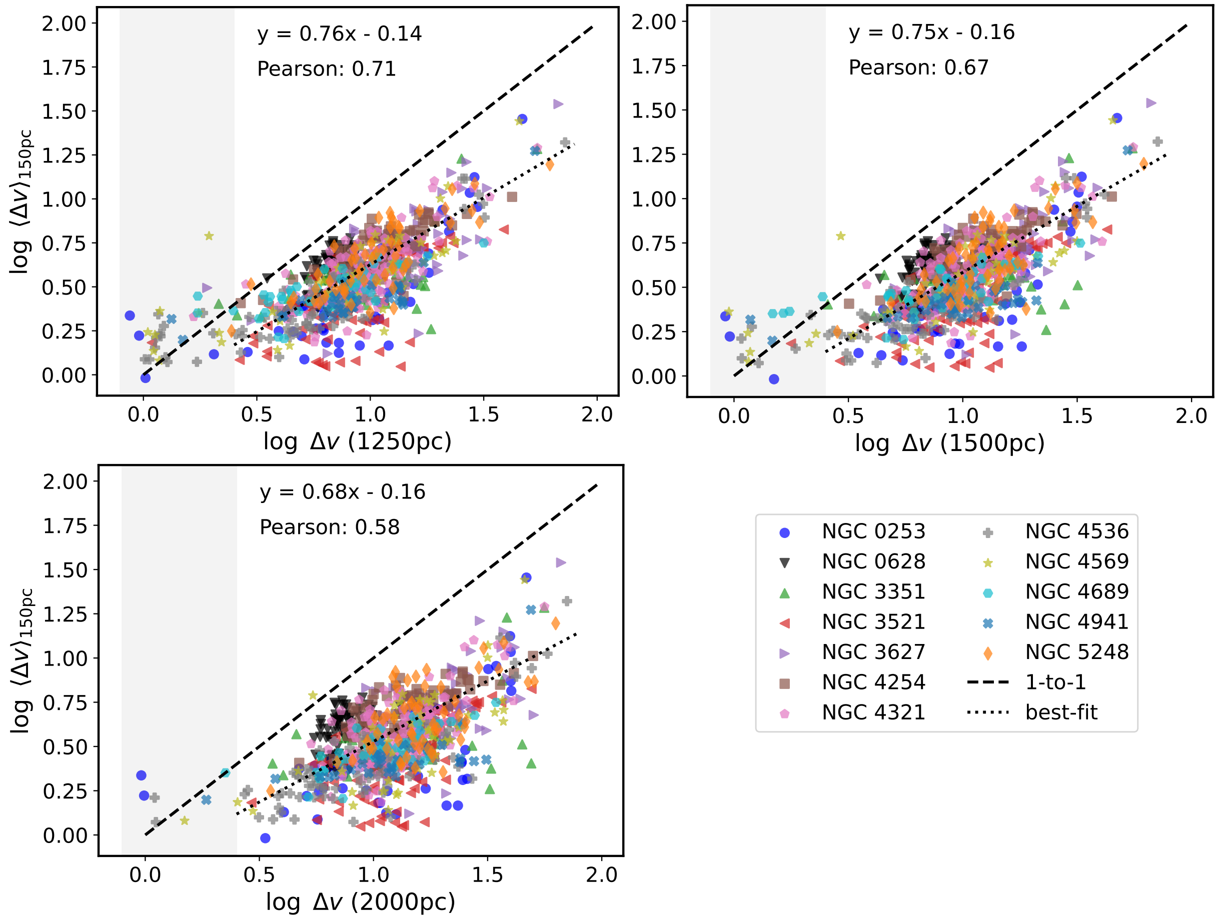

Figure 2. The 1.5-kpc-averaged intensity-weighted velocity dispersion at 150-pc scales ($\langle\Delta v\rangle_{\rm 150pc}$; J. Sun et al. 2022) strongly correlates with lower-resolution Δv measured directly on kpc scales. This implies that kpc-scale Δv can still be a good tracer for near-GMC-scale Δv at 150-pc resolutions. The dashed lines represent a 1-to-1 relation, and the dotted lines show the best-fit linear function (in log scale) as annotated on each panel. The shaded areas indicate regimes below the data spectral resolution of 2.5 km s^{-1}, which we exclude in our fitting. The decreasing slope and correlation with scales suggests diminishing contribution from GMC-scale motions and may support a picture of hierarchical, turbulent molecular clouds up to kpc scales.

ment verifies our approach to separate gas motions within and beyond 150-pc scales, supports our finding that intra-cloud motions play a critical role in kpc-scale Δv measurements (more discussions in §4.1), and thus explains why the Δv-based $\alpha_{\rm CO}$ prescription can be extended from ∼100-pc to kpc scales.

3.3. $\alpha_{\rm CO}$ *Dependence on the* CO/^{13}CO *Line Ratio*

In addition to CO velocity dispersion, recent GMC-scale observations of barred galaxies and/or starbursts have revealed significant $\alpha_{\rm CO}$ variations which correlate well with the ^{12}CO/^{13}CO line ratios ($R_{12/13}$; Y.-H. Teng et al. 2023; H. He et al. 2024; J. den Brok et al. 2025a), implying that $R_{12/13}$ also tracks CO opacity changes and $\alpha_{\rm CO}$ well. Previous studies have also shown evidence that $R_{12/13}$ correlates inversely with CO opacity (M. J. Jiménez-Donaire et al. 2017; D. Cormier et al. 2018; F. P. Israel 2020; K. Morokuma-Matsui et al. 2020).

To investigate whether the $\alpha_{\rm CO}$-$R_{12/13}$ correlation extends to kpc scales and/or applies to broader galactic environments (e.g., unbarred galaxies), we use 1.5-kpc-scale ^{12}CO and ^{13}CO (1–0) observations from the COMING survey (K. Sorai et al. 2019) and explore how their $R_{12/13}$ varies with the 2-kpc-scale $\alpha_{\rm CO}$ measurements from I.-D. Chiang et al. (2024). These studies have 7 common galaxies, including 2 barred (NGC 3627 and 4258) and 5 unbarred (NGC 0628, 2841, 3938, 4030, and 7331). However, we note that $R_{12/13}$ from these data is likely biased toward the brightest regions in the galaxies (due to limited sensitivity; §2.3), and that our work here is simply an initial attempt to explore $R_{12/13}$ as a potential $\alpha_{\rm CO}$ indicator for kpc-scale CO observations.

Figure 4b presents an overall decreasing $\alpha_{\rm CO}$ trend with $R_{12/13}$ across the 7 galaxies. The colored points are data with S/N $>$ 3 in both ^{12}CO and ^{13}CO, and the gray triangles show data with S/N $>$ 3 in ^{12}CO but

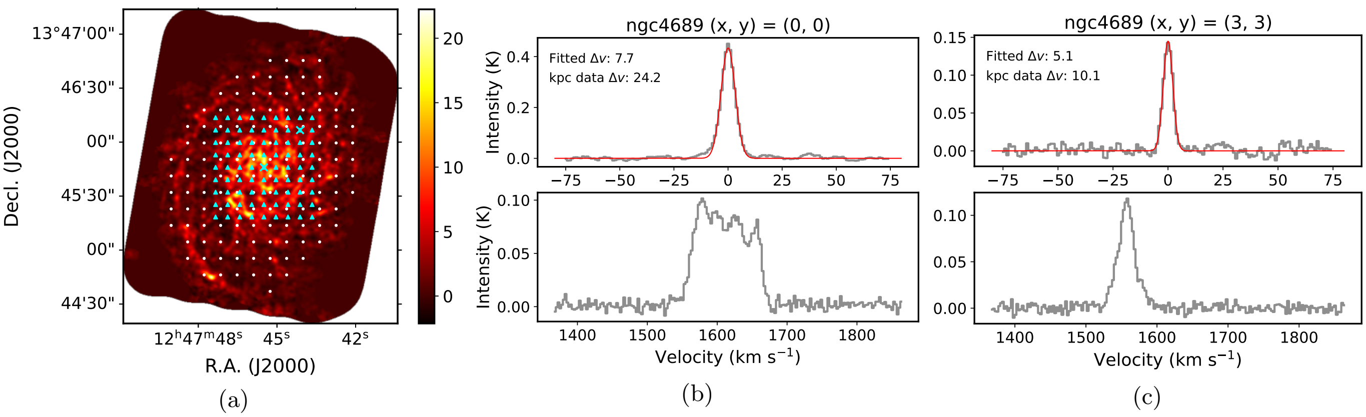

Figure 3. Demonstration of the cross-resolution Δv sampling and analysis in §3.2.2, here showing NGC 4689 as an example. (a) The CO (2–1) moment-0 map of NGC 4689 at 150-pc resolutions, overlaid with white and cyan points indicating the sampled positions of dust-based $\alpha_{\rm CO}$ measurements and the center positions of kpc-sized squares for spectral stacking, respectively. (b, c) Representative spectra at the (b) center and (c) disk positions, as labeled by the two cyan crosses in (a). The top panels show the moment-1-centered and stacked spectra averaged over the kpc-sized aperture (overlaid with best-fit Gaussian curves), aiming to remove dynamical effects beyond 150-pc scales. The bottom panels represent directly stacked spectra from kpc-scale data. The best-fit Gaussian Δv for the upper panels and the mean kpc-scale Δv (both in km s^{-1}) are annotated on the upper left corners, which generally differ within a factor of two (e.g., panel c) except in central apertures (panel b).

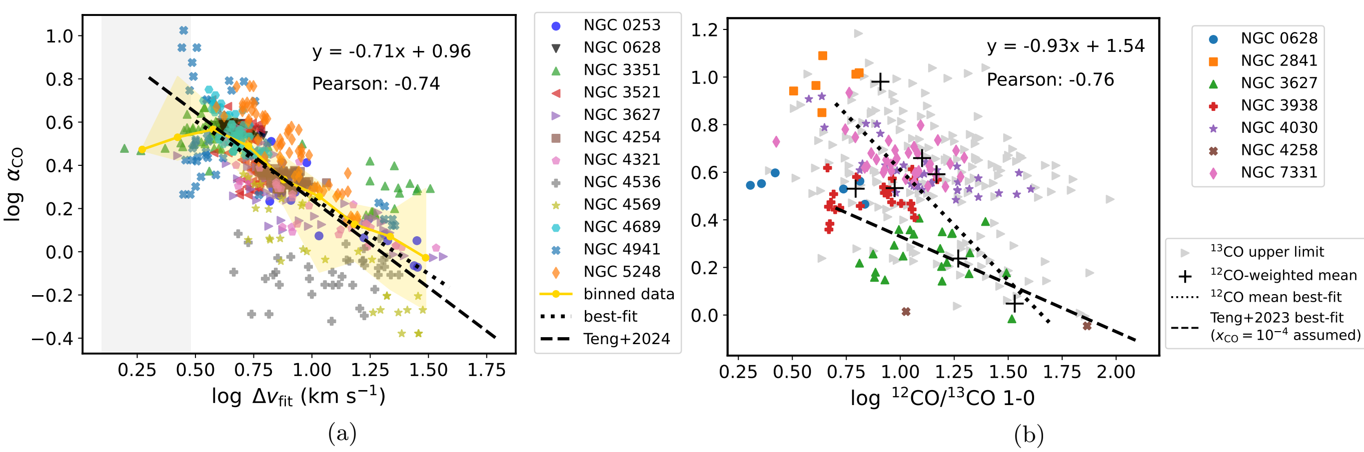

Figure 4. (a) $\alpha_{\rm CO}$ anti-correlates with the fitted $\Delta v_{\rm 150pc}$ after excluding large-scale ($>$ 150-pc) motions across kpc-scale apertures, agreeing well with the Y.-H. Teng et al. (2024) prescription shown by the dashed line. The yellow line and shading represent the binned medians and 16$^{\rm th}$–84$^{\rm th}$ percentile range of $\alpha_{\rm CO}$, respectively. The dotted line and the equation on the upper right corner indicate the best-fit relation. (b) $\alpha_{\rm CO}$ also shows a mild anti-correlation with the ^{12}CO/^{13}CO line ratio measured at kpc resolutions, while much of the data is limited by S/N < 3 in ^{13}CO (gray triangles). The plus signs (with a best-fit relation shown by the dotted line) represent the integrated $R_{12/13}$ of each galaxy and the global mean $\alpha_{\rm CO}$ weighted by ^{12}CO intensities. The barred galaxies agree well with the trend of nearby barred galaxy centers in Y.-H. Teng et al. (2023).

< 3 in ^{13}CO. We also derive galaxy-integrated $R_{12/13}$ by including all the pixels with S/N > 1 in ^{13}CO. The integrated $R_{12/13}$ values and the ^{12}CO-intensity-weighted mean of $\alpha_{\rm CO}$ (plus signs) also form a decreasing $\alpha_{\rm CO}$-$R_{12/13}$ trend, with a Pearson coefficient of -0.76 and a p-value of 0.045. The best-fit relation (dotted line) of these integrated data is $\log(\alpha_{\rm CO}) = (-0.93 \pm 0.35) \cdot \log(R_{12/13}) + (1.54 \pm 0.40)$.

All the barred galaxies show lower $\alpha_{\rm CO}$ values than unbarred galaxies, which may be explained by substantial CO line broadening near barred galaxy centers due to increased streaming motions and/or bar-driven inflows (Y.-H. Teng et al. 2022, 2023). The different $\alpha_{\rm CO}$ ranges between barred and unbarred galaxies may indicate an existence of separate $\alpha_{\rm CO}$-$R_{12/13}$ relations for the two populations, but could also originate from incomplete spatial coverage due to limited data sensitivity. Notably, the two barred galaxies also align well with previous GMC-scale studies of barred galaxies, including three nearby galaxy centers (Y.-H. Teng et al. 2023) and M51 (J. den Brok et al. 2025a), assuming a

CO/H_2 abundance ratio of $x_{\rm CO} = 10^{-4}$ as suggested in Y.-H. Teng et al. (2024).

Overall, the observed $\alpha_{\rm CO}$-$R_{12/13}$ anti-correlation and its agreement with previous studies suggest that $R_{12/13}$ could also be useful as a cross-scale $\alpha_{\rm CO}$ indicator complementing Δv. However, we note again that the current dataset are limited in sensitivity and sample size, and thus future studies with systematic and sensitive ^{13}CO observations will be required for further verification.

4. DISCUSSION

§3.1 reveals clear anti-correlations between kpc-scale $\alpha_{\rm CO}$ and CO velocity dispersion from ∼100-pc to 2-kpc resolutions across 12 galaxies from the PHANGS-ALMA survey. Such a cross-scale Δv-dependent $\alpha_{\rm CO}$ prescription can be explained by the strong correlations between $\Delta v_{\rm 150pc}$ and kpc-scale Δv (§3.2.1), suggesting that kpc-scale Δv can track 150-pc-scale Δv well with a scale-dependent offset. We further verify that $\Delta v_{\rm 150pc}$ does contribute significantly on kpc scales, by separating line profiles contributed from within and beyond 150-pc scales via moment-1-centered spectral stacking (§3.2.2).

4.1. *Internal or External Cloud Motions?*

To understand the rationale behind Δv-dependent $\alpha_{\rm CO}$ prescriptions, it is important to know whether the observed Δv traces gas motions internal or external to molecular clouds, as intra-cloud (internal) and inter-cloud (external) dynamics originate from different physical processes (J. H. Orkisz et al. 2017; Y.-H. Teng & N. Hirano 2020; S. M. R. Jeffreson et al. 2022; E. Schinnerer et al. 2023). With a physical resolution of 150 pc, our CO data already probe a scale near the size of GMCs (e.g., S. E. Ragan et al. 2014; J. E. Großschedl et al. 2018). However, as most molecular clouds are smaller than GMCs, it is likely that $\Delta v_{\rm 150pc}$ contains more inter-cloud motions than intra-cloud motions, especially in spectrally complex regions such as galaxy centers (J. D. Henshaw et al. 2026, in preparation).

With the current dataset, we are not able to resolve inter- and intra-cloud motions below 150-pc scales. Nonetheless, the fact that $\alpha_{\rm CO}$ correlates well with $\Delta v_{\rm 150pc}$ (Y.-H. Teng et al. 2024) and extends all the way up to $\Delta v_{\rm 2kpc}$ (this work) provides several possible interpretations. First, if $\Delta v_{\rm 150pc}$ is indeed tracing the intra-cloud motions, then it means that intra-cloud motions contribute significantly even in kpc-scale Δv. This further indicates that the $\alpha_{\rm CO}$ variation with Δv is mainly caused by intrinsic molecular cloud turbulence that alter the CO optical depths (P. P. Papadopoulos et al. 2012; Y.-H. Teng et al. 2022, 2023; H. He et al. 2024), which would also explain the observed $\alpha_{\rm CO}$-$R_{12/13}$ anti-correlation in §3.3.

Even if $\Delta v_{\rm 150pc}$ is dominated by inter-cloud motions, the magnitude of intra- and inter-cloud motions on kpc scales may still be well-correlated if they are under the same hierarchical structure of turbulence (B. G. Elmegreen & Y. N. Efremov 1996; O. Agertz et al. 2015; M. Nandakumar & P. Dutta 2023), which could lead to a $\Delta v \sim \ell^{0.3-0.5}$ scaling similar to the Δv offset with scales (ℓ) in Figure 2. This also implies that the contribution from truly non-turbulence (e.g., orbital, streaming) motions is small over most kpc-sized areas.

Alternatively, the $\alpha_{\rm CO}$ dependence on Δv could also be driven by non-dynamical properties correlated with the large-scale Δv between molecular clouds and the galaxy, such as temperature and/or CO excitation (D. Narayanan et al. 2012; A. D. Bolatto et al. 2013; M. Gong et al. 2020), molecular gas surface densities (J. Sun et al. 2022), or CO-dark gas fraction (G. Accurso et al. 2017; S. C. Madden et al. 2020). These properties may also correlate with $R_{12/13}$, which is known to be driven by changes in both the CO optical depth and CO isotopologue abundance ratio.

Regardless of whether $\Delta v_{\rm 150pc}$ traces internal or external cloud dynamics, the $\alpha_{\rm CO}$-Δv relationship from ∼100-pc to 2-kpc scales can be useful for galaxy studies to obtain accurate molecular mass and star formation properties. However, we add a caveat that all of our galaxy sample comes from PHANGS, which focuses on relatively face-on star-forming disk galaxies. It is likely that different types of galaxies (e.g., irregular, interacting, high-z) exhibit more complicated gas kinematics such that their $\alpha_{\rm CO}$-Δv relationship differs from our results. In §4.2, we will compare our results to current $\alpha_{\rm CO}$ studies and discuss the realm of usefulness for our cross-scale $\alpha_{\rm CO}$ prescriptions.

4.2. *Application of Current $\alpha_{\rm CO}$ Prescriptions*

Our finding of strong anti-correlations between $\alpha_{\rm CO}$ and CO velocity dispersion from ∼100-pc to 2-kpc scales (§3.1), as well as $\alpha_{\rm CO}$ variations with $R_{12/13}$ at 1.5-kpc scale (§3.3), can be systematically used in galaxy studies to infer molecular gas mass and properties from CO observations. These CO-based $\alpha_{\rm CO}$ prescriptions, requiring only the CO data, are convenient and straightforward to implement. The CO line properties also have the advantage of directly tracking the molecular gas conditions that physically drive $\alpha_{\rm CO}$ variations (e.g., opacity changes; §4.1), thereby leading to a scatter less than ±0.2 dex in our extended Δv-based prescriptions (see Figure 1). However, we note that our sample of galaxies spans a small metallicity range within 0.3 dex below the solar value (Y.-H. Teng et al. 2024), and thus these prescriptions may only apply to moderate to near-solar metallicity regions, where low-metallicity effects on α_{CO} become secondary (L. K. Hunt et al. 2015; C.-Y. Hu et al. 2022).

The originally proposed Δv-dependent α_{CO} prescription, despite its requirement of high-resolution ($\lesssim$150 pc) data, reveals a high α_{CO} precision with $\sim$0.1 dex scatter (Y.-H. Teng et al. 2024). In addition, it has been useful for revealing GMC-scale physics in recent galaxy studies (e.g., J. Kim et al. 2026; M. Sánchez-García et al. 2026). Other follow-up studies have also verified a similar α_{CO}-Δv anti-correlation across more nearby star-forming galaxies, including luminous infrared galaxies (A. R. Bemis et al. 2024; H. He et al. 2024; J. den Brok et al. 2025a). With the α_{CO}-Δv relation being extended to 2-kpc scales, such Δv-based prescription becomes even more practical, as it can be applied to more galaxy surveys with kpc-scale CO observations, including HERACLES (A. K. Leroy et al. 2009), EDGE (A. D. Bolatto et al. 2017; V. Villanueva et al. 2024; Y.-H. Teng et al. 2026), COMING (K. Sorai et al. 2019), ALMaQUEST (L. Lin et al. 2020), ALMA-FACTS (J. Koda et al. 2026, submitted), KILOGAS (T. A. Davis & KILOGAS team 2026, in preparation), and potentially also to higher redshifts (e.g., F. Rizzo et al. 2023).

With CO data at $\sim$kpc resolutions, it is recently common to adopt α_{CO} prescriptions that depend on metallicity and/or stellar mass surface density (A. D. Bolatto et al. 2013; G. Accurso et al. 2017; I.-D. Chiang et al. 2024; E. Schinnerer & A. K. Leroy 2024). The estimated uncertainty of these prescriptions is typically $\pm$0.3 dex (e.g., A. D. Bolatto et al. 2013), and deriving metallicity or stellar mass density requires ancillary data additional to CO. However, not all galaxies have available multi-band observations for deriving those quantities, and it can also be difficult to obtain such observations in some galactic environments. For instance, quenched or quiescent galaxies below the star formation main sequence can have many retired regions with low star formation rates, where the ionized line emission no longer probes ionization driven by radiation from young massive stars (L. Lin et al. 2022; D. Colombo et al. 2025; T. G. Williams et al. 2025; Y.-H. Teng et al. 2026). This would disable the use of metallicity calibrations based on strong ionized lines (e.g., M. Pettini & B. E. J. Pagel 2004; L. S. Pilyugin & E. K. Grebel 2016; M. Curti et al. 2017). In such cases, the kpc-scale Δv-based α_{CO} prescription would be helpful for estimating molecular gas properties more accurately than assuming a constant α_{CO}. The Δv-dependent α_{CO} prescription would also be useful for studying dynamics-related properties of molecular gas in galaxies, including the star formation efficiency and dynamical equilibrium pressure (e.g., S. L. Ellison et al. 2024; A. K. Leroy et al. 2025).

Finally, we note that current α_{CO} prescriptions (including this work) are mostly calibrated on nearby star-forming galaxies around or above the main sequence. This is because measuring α_{CO} in quenched or low-surface-density galaxies remains challenging due to their general lack of molecular gas. It is also important to note that our galaxy samples have metallicity $\gtrsim 0.6\ Z_{\odot}$, and thus their α_{CO} variation is not dominated by the lack of dust shielding due to poor amount of CO (Y.-H. Teng et al. 2024), which are typically found in low-mass, metal-poor dwarf galaxies (e.g., M. Rubio et al. 2015; V. Villanueva et al. 2025). To test if our prescription can be extended to low-metallicity galaxies or more dynamically complex systems, it requires future studies with systematic α_{CO} measurements in those environments.

5. CONCLUSIONS

We investigate the relationship between CO-to-H_2 conversion factor (α_{CO}) and CO line properties across 12 nearby galaxies with spatial resolutions varied up to 2-kpc scales, expanding upon recent GMC-scale studies (Y.-H. Teng et al. 2023, 2024). The establishment of these cross-scale α_{CO} prescriptions would improve the estimation of α_{CO} and molecular gas properties in kpc-scale galaxy observations, complementing previous prescriptions based on indirect tracers of molecular gas. Our main results are summarized as follows:

1. We find clear anti-correlations between α_{CO} and inclination-corrected CO velocity dispersion (Δv) across resolutions ranging from 250 pc to 2 kpc, with a typical 1-σ scatter of 0.2 dex (§3.1). The best-fit power-law slopes for these relations are $\sim$0.8, agreeing well with previously established relations at 150-pc scales (Y.-H. Teng et al. 2024). The intercept of the relation increases with the resolution scale, indicating increased Δv due to larger-scale motions within larger beam sizes.

2. The viability of the cross-scale α_{CO}-Δv relationship (Table 1) is due to strong correlations between Δv measured at both 150-pc scales and at lower physical resolutions up to 2 kpc (§3.2.1). By employing moment-1-centered spectral stacking, we further verify that gas motions within 150-pc scales make a key contribution to kpc-scale Δv across the galaxy disks (§3.2.2).

3. We also observe an overall decreasing trend between the 2-kpc-scale α_{CO} measurements (from I.-D. Chiang et al. 2024) and the 1.5-kpc-scale

^{12}CO/^{13}CO line ratio ($R_{12/13}$) from COMING (K. Sorai et al. 2019) across 7 galaxies (§3.3). The barred galaxies in the sample align well with previous GMC-scale studies (Y.-H. Teng et al. 2023). This suggests that $R_{12/13}$ could also be a cross-scale $\alpha_{\rm CO}$ indicator, though further verification with sensitive ^{13}CO observations is required.

4. Depending on whether Δv at 150 pc scales tracks intra-cloud or inter-cloud motions, the precise physical driver of the Δv-based $\alpha_{\rm CO}$ prescription may be rooted in 1) internal cloud dynamics that alters CO opacity, either directly or through a hierarchical turbulence cascade; or 2) galactic-scale dynamics that reflect other Δv-correlated properties. Higher-resolution observations are required to disentangle the intra-cloud and inter-cloud dynamics below 150-pc scales.

In summary, the accuracy and broadened applicability of Δv-based $\alpha_{\rm CO}$ prescriptions (with an inclination correction) provide a reliable and robust framework for determining molecular gas masses within star-forming galaxies. In particular, this cross-scale prescription can be highly practical for kpc-scale galaxy surveys, especially in environments where conventional $\alpha_{\rm CO}$ prescriptions may fail. Our exploration of the $\alpha_{\rm CO}$ dependence on $R_{12/13}$ also shows its potential to be extended to kpc scales and/or broader galactic environments, but high-quality CO isotopologue observations toward a more diverse galaxy sample will be needed to confirm.

This work was carried out as part of the PHANGS collaboration. Y.-H.T thanks Dr. Kazuyuki Muraoka for helpful discussions on the COMING data. Y.-H.T. and A.D.B. acknowledge funding support from the National Science Foundation (NSF) under grant No. 2307441. A.U. acknowledges support from the Spanish grant PID2022-138560NB-I00, funded by MCIN/AEI/10.13039/501100011033/FEDER, EU. D.C. gratefully acknowledges the Collaborative Research Center 1601 (SFB 1601 sub-project B3) funded by the Deutsche Forschungsgemeinschaft (DFG, German Research Foundation) – 500700252. H.-A.P. acknowledges support from the National Science and Technology Council of Taiwan under grant 113-2112-M-032-014-MY3. V.V. acknowledges support from the Comité ESO Mixto 2024 and from the ANID BASAL project FB210003. TGW gratefully acknowledges support from the UK ALMA Regional Centre (ARC) Node, which is supported by the Science and Technology Facilities Council grant number ST/Y004108/1.

This paper makes use of the following ALMA data:
ADS/JAO.ALMA#2012.1.00650.S,
ADS/JAO.ALMA#2013.1.00803.S,
ADS/JAO.ALMA#2013.1.01161.S,
ADS/JAO.ALMA#2015.1.00925.S,
ADS/JAO.ALMA#2015.1.00956.S,
ADS/JAO.ALMA#2017.1.00392.S,
ADS/JAO.ALMA#2017.1.00766.S,
ADS/JAO.ALMA#2017.1.00886.L,
ADS/JAO.ALMA#2018.1.01321.S,
ADS/JAO.ALMA#2018.1.01651.S.
ADS/JAO.ALMA#2018.A.00062.S.
ALMA is a partnership of ESO (representing its member states), NSF (USA) and NINS (Japan), together with NRC (Canada), NSTC and ASIAA (Taiwan), and KASI (Republic of Korea), in cooperation with the Republic of Chile. The Joint ALMA Observatory is operated by ESO, AUI/NRAO and NAOJ. The National Radio Astronomy Observatory and Green Bank Observatory are facilities of the U.S. National Science Foundation operated under cooperative agreement by Associated Universities, Inc.

This work is based in part on data products from the Wide-field Infrared Survey Explorer (E. L. Wright et al. 2010), which is a joint project of the University of California, Los Angeles, and the Jet Propulsion Laboratory/California Institute of Technology, funded by the National Aeronautics and Space Administration. This work is also based partially on published data from the Nobeyama 45 m radio telescope, which is operated by Nobeyama Radio Observatory, a branch of National Astronomical Observatory of Japan. We acknowledge the usage of the SAO/NASA Astrophysics Data System.

Facilities: ALMA, WISE, Herschel, VLA, NRO 45m

Software: `spectral-cube` (A. Ginsburg et al. 2019), `matplotlib` (J. D. Hunter 2007), `numpy` (C. R. Harris et al. 2020), `scipy` (P. Virtanen et al. 2020), `astropy` (Astropy Collaboration et al. 2022), `ipython` (F. Pérez & B. E. Granger 2007)

APPENDIX

Table 2. Statistics of 150-pc and 1-kpc Δv across Galaxies

Galaxy	Center			Disk				
	$\Delta v_{\rm kpc}$	$\Delta v_{\rm 150pc}$	$\frac{\Delta v_{\rm 150pc}}{\Delta v_{\rm kpc}}$	$\mu(\Delta v_{\rm kpc})$	$\sigma(\Delta v_{\rm kpc})$	$\mu(\Delta v_{\rm 150pc})$	$\sigma(\Delta v_{\rm 150pc})$	$\mu(\frac{\Delta v_{\rm 150pc}}{\Delta v_{\rm kpc}})$
	[km s^{-1}]	[km s^{-1}]		[km s^{-1}]	[km s^{-1}]	[km s^{-1}]	[km s^{-1}]	
(1)	(2)	(3)	(4)	(5)	(6)	(7)	(8)	(9)
NGC0253	86.33	58.95	68.28%	37.65	18.33	21.33	14.21	56.67%
NGC0628	10.21	5.60	54.81%	7.03	1.16	4.82	0.61	68.59%
NGC3351	49.99	21.90	43.81%	15.98	10.76	10.11	11.19	63.28%
NGC3521	50.04	11.96	23.89%	28.47	8.07	9.34	1.00	32.79%
NGC3627	75.37	49.18	65.25%	28.17	12.79	15.28	10.83	54.23%
NGC4254	33.19	11.72	35.31%	18.45	5.18	10.52	6.62	56.99%
NGC4321	48.32	27.50	56.92%	22.59	8.38	20.67	10.33	91.52%
NGC4536	83.53	37.03	44.33%	31.93	17.97	14.42	10.71	45.15%
NGC4569	70.98	51.15	72.06%	30.00	13.88	15.55	10.75	51.85%
NGC4689	24.16	7.72	31.97%	12.60	3.53	5.12	1.31	40.64%
NGC4941	64.82	27.88	43.00%	17.77	10.88	6.76	7.25	38.03%
NGC5248	54.06	19.03	35.21%	24.22	10.32	10.24	3.82	42.27%
Overall	$52.05^{+20.03}_{-7.51}$	$24.70^{+15.37}_{-12.80}$	$44.07\%^{+14.93\%}_{-8.78\%}$	$23.40^{+5.45}_{-6.08}$	$10.54^{+2.52}_{-3.19}$	$10.38^{+4.97}_{-1.68}$	$8.79^{+1.98}_{-5.60}$	$53.04\%^{+11.18\%}_{-5.52\%}$

Note—(1) Galaxy name; (2–4) measured Δv based on 1-kpc data, stacked 150-pc line profiles, and their ratios in the central 1-kpc aperture; (5–6) mean and standard deviation of the measured Δv across all kpc-sized apertures on galaxy disks (excluding the central apertures), based on 1-kpc data or (7–8) the stacked 150-pc line profiles; (9) mean ratio of $\Delta v_{\rm 150pc}/\Delta v_{\rm kpc}$ for all kpc-sized apertures on galaxy disks. The overall statistics (bottom row) indicates the median $\pm\ \sigma$ values based on the 16$^{\rm th}$, 50$^{\rm th}$, and 84$^{\rm th}$ percentile values across all galaxies. All Δv values in this table are not corrected for galaxy inclination.

A. STATISTICS FROM MULTI-SCALE ΔV MEASUREMENTS

In §3.2.2, we report that gas motions within 150-pc scales (as inferred from $\Delta v_{\rm 150pc}$) can still be significant in kpc-scale measurements (as inferred from $\Delta v_{\rm kpc}$). Here we provide the supporting statistics from our Δv measurements. Table 2 lists the measured $\Delta v_{\rm 150pc}$ and $\Delta v_{\rm kpc}$ over the central and disk apertures across all 12 galaxies. Overall, the central kpc regions of galaxies show the highest Δv in a galaxy due to strong beam smearing from galaxy rotation. Additionally, galaxy centers tend to show $\Delta v_{\rm 150pc}$ lower than 50% of $\Delta v_{\rm kpc}$, with a median of 44% and a 16$^{\rm th}$–84$^{\rm th}$ percentile range of 35%–59%. On the other hand, $\Delta v_{\rm 150pc}$ is generally more than 50% of $\Delta v_{\rm kpc}$ across galaxy disks, showing a median of 53% and a 16$^{\rm th}$–84$^{\rm th}$ percentile range of 48%–64%.

Among all 12 galaxies, NGC 3521 shows the lowest $\Delta v_{\rm 150pc}/\Delta v_{\rm kpc}$ ratio of $\sim$30%, which could be due to its high inclination ($i \sim 70°$) that would blend in more large-scale motion along a sightline. However, we do not observe a similarly low ratio in NGC 0253 with $i \sim 75°$ (A. K. Leroy et al. 2021a). This may be explained by the high uncertainty in effective line widths or moment-based dispersions due to high spectral complexity in highly-inclined galaxy centers (J. D. Henshaw et al. 2026, in preparation). We note that all the Δv reported here are pure line-of-sight measurements without accounting for galaxy inclinations, as we are interested in the ratios between different scales. However, the $\alpha_{\rm CO}$-Δv relations in §3.1 does require an additional $\sqrt{\cos i}$ factor for inclination correction, which ranges from a factor 0.5 (NGC 0253) to 1.0 (NGC 0628) for our sample.

REFERENCES

Accurso, G., Saintonge, A., Catinella, B., et al. 2017, MNRAS, 470, 4750, doi: 10.1093/mnras/stx1556

Agertz, O., Romeo, A. B., & Grisdale, K. 2015, MNRAS, 449, 2156, doi: 10.1093/mnras/stv440

Astropy Collaboration, Price-Whelan, A. M., Lim, P. L., et al. 2022, ApJ, 935, 167, doi: 10.3847/1538-4357/ac7c74

Bemis, A. R., Wilson, C. D., Sharda, P., Roberts, I. D., & He, H. 2024, A&A, 692, A146, doi: 10.1051/0004-6361/202347879

Bolatto, A. D., Wolfire, M., & Leroy, A. K. 2013, ARA&A, 51, 207, doi: 10.1146/annurev-astro-082812-140944

Bolatto, A. D., Wong, T., Utomo, D., et al. 2017, ApJ, 846, 159, doi: 10.3847/1538-4357/aa86aa

Calistro Rivera, G., Hodge, J. A., Smail, I., et al. 2018, ApJ, 863, 56, doi: 10.3847/1538-4357/aacffa

Chiang, I.-D., Sandstrom, K. M., Chastenet, J., et al. 2024, ApJ, 964, 18, doi: 10.3847/1538-4357/ad23ed

Colombo, D., Kalinova, V., Bazzi, Z., et al. 2025, A&A, 699, A366, doi: 10.1051/0004-6361/202453179

Cormier, D., Bigiel, F., Jiménez-Donaire, M. J., et al. 2018, MNRAS, 475, 3909, doi: 10.1093/mnras/sty059

Curti, M., Cresci, G., Mannucci, F., et al. 2017, MNRAS, 465, 1384, doi: 10.1093/mnras/stw2766

Davis, T. A., & KILOGAS team. 2026

den Brok, J., Jiménez-Donaire, M. J., Leroy, A., et al. 2025a, AJ, 169, 18, doi: 10.3847/1538-3881/ad888a

den Brok, J., Oakes, E. K., Leroy, A. K., et al. 2025b, ApJ, 988, 162, doi: 10.3847/1538-4357/addf4c

Ellison, S. L., Pan, H.-A., Bluck, A. F. L., et al. 2024, MNRAS, 527, 10201, doi: 10.1093/mnras/stad3778

Elmegreen, B. G., & Efremov, Y. N. 1996, ApJ, 466, 802, doi: 10.1086/177554

Ginsburg, A., Koch, E., Robitaille, T., et al. 2019, radio-astro-tools/spectral-cube: Release v0.4.5, v0.4.5 Zenodo, doi: 10.5281/zenodo.3558614

Girichidis, P., Offner, S. S. R., Kritsuk, A. G., et al. 2020, SSRv, 216, 68, doi: 10.1007/s11214-020-00693-8

Gong, M., Ostriker, E. C., Kim, C.-G., & Kim, J.-G. 2020, ApJ, 903, 142, doi: 10.3847/1538-4357/abbdab

Großschedl, J. E., Alves, J., Meingast, S., et al. 2018, A&A, 619, A106, doi: 10.1051/0004-6361/201833901

Harris, C. R., Millman, K. J., van der Walt, S. J., et al. 2020, Nature, 585, 357, doi: 10.1038/s41586-020-2649-2

He, H., Wilson, C. D., Sun, J., et al. 2024, ApJ, 971, 176, doi: 10.3847/1538-4357/ad5544

Henshaw, J. D., Leroy, A. K., Rosolowsky, E., et al. 2026

Hu, C.-Y., Schruba, A., Sternberg, A., & van Dishoeck, E. F. 2022, ApJ, 931, 28, doi: 10.3847/1538-4357/ac65fd

Hunt, L. K., García-Burillo, S., Casasola, V., et al. 2015, A&A, 583, A114, doi: 10.1051/0004-6361/201526553

Hunter, J. D. 2007, Computing In Science & Engineering, 9, 90

Israel, F. P. 2020, A&A, 635, A131, doi: 10.1051/0004-6361/201834198

Jeffreson, S. M. R., Sun, J., & Wilson, C. D. 2022, MNRAS, 515, 1663, doi: 10.1093/mnras/stac1874

Jiménez-Donaire, M. J., Bigiel, F., Leroy, A. K., et al. 2017, MNRAS, 466, 49, doi: 10.1093/mnras/stw2996

Kim, J., Leroy, A. K., Sandstrom, K., et al. 2026, ApJ, 1001, 67, doi: 10.3847/1538-4357/ae4599

Klessen, R. S., & Glover, S. C. O. 2016, Saas-Fee Advanced Course, 43, 85, doi: 10.1007/978-3-662-47890-5_2

Koda, J., A, B, C, & D. 2026

Kohno, M., & Sofue, Y. 2024, MNRAS, 527, 9290, doi: 10.1093/mnras/stad3648

Krumholz, M. R. 2014, PhR, 539, 49, doi: 10.1016/j.physrep.2014.02.001

Larson, R. B. 1981, MNRAS, 194, 809, doi: 10.1093/mnras/194.4.809

Leroy, A. K., Walter, F., Bigiel, F., et al. 2009, AJ, 137, 4670, doi: 10.1088/0004-6256/137/6/4670

Leroy, A. K., Schinnerer, E., Hughes, A., et al. 2021a, ApJS, 257, 43, doi: 10.3847/1538-4365/ac17f3

Leroy, A. K., Hughes, A., Liu, D., et al. 2021b, ApJS, 255, 19, doi: 10.3847/1538-4365/abec80

Leroy, A. K., Rosolowsky, E., Usero, A., et al. 2022, ApJ, 927, 149, doi: 10.3847/1538-4357/ac3490

Leroy, A. K., Sun, J., Meidt, S., et al. 2025, ApJ, 985, 14, doi: 10.3847/1538-4357/adbcab

Lin, L., Ellison, S. L., Pan, H.-A., et al. 2020, ApJ, 903, 145, doi: 10.3847/1538-4357/abba3a

Lin, L., Ellison, S. L., Pan, H.-A., et al. 2022, ApJ, 926, 175, doi: 10.3847/1538-4357/ac4ccc

Madden, S. C., Cormier, D., Hony, S., et al. 2020, A&A, 643, A141, doi: 10.1051/0004-6361/202038860

McKee, C. F., & Ostriker, E. C. 2007, ARA&A, 45, 565, doi: 10.1146/annurev.astro.45.051806.110602

Morokuma-Matsui, K., Sorai, K., Sato, Y., et al. 2020, PASJ, 72, 90, doi: 10.1093/pasj/psaa084

Nandakumar, M., & Dutta, P. 2023, MNRAS, 526, 4690, doi: 10.1093/mnras/stad3042

Narayanan, D., Krumholz, M. R., Ostriker, E. C., & Hernquist, L. 2012, MNRAS, 421, 3127, doi: 10.1111/j.1365-2966.2012.20536.x

Orkisz, J. H., Pety, J., Gerin, M., et al. 2017, A&A, 599, A99, doi: 10.1051/0004-6361/201629220

Paglione, T. A. D., Wall, W. F., Young, J. S., et al. 2001, ApJS, 135, 183, doi: 10.1086/321785

Papadopoulos, P. P., van der Werf, P., Xilouris, E., Isaak, K. G., & Gao, Y. 2012, ApJ, 751, 10, doi: 10.1088/0004-637X/751/1/10

Pérez, F., & Granger, B. E. 2007, Computing in Science and Engineering, 9, 21, doi: 10.1109/MCSE.2007.53

Pettini, M., & Pagel, B. E. J. 2004, MNRAS, 348, L59, doi: 10.1111/j.1365-2966.2004.07591.x

Pilyugin, L. S., & Grebel, E. K. 2016, MNRAS, 457, 3678, doi: 10.1093/mnras/stw238

Pineda, J. E., Caselli, P., & Goodman, A. A. 2008, ApJ, 679, 481, doi: 10.1086/586883

Ragan, S. E., Henning, T., Tackenberg, J., et al. 2014, A&A, 568, A73, doi: 10.1051/0004-6361/201423401

Renaud, F., Bournaud, F., Daddi, E., & Weiß, A. 2019, A&A, 621, A104, doi: 10.1051/0004-6361/201834397

Rizzo, F., Roman-Oliveira, F., Fraternali, F., et al. 2023, A&A, 679, A129, doi: 10.1051/0004-6361/202346444

Rubio, M., Elmegreen, B. G., Hunter, D. A., et al. 2015, Nature, 525, 218, doi: 10.1038/nature14901

Sánchez-García, M., Díaz-Santos, T., Barcos-Muñoz, L., et al. 2026, A&A, 707, A144, doi: 10.1051/0004-6361/202555198

Sandstrom, K. M., Leroy, A. K., Walter, F., et al. 2013, ApJ, 777, 5, doi: 10.1088/0004-637X/777/1/5

Schinnerer, E., & Leroy, A. K. 2024, ARA&A, 62, 369, doi: 10.1146/annurev-astro-071221-052651

Schinnerer, E., Emsellem, E., Henshaw, J. D., et al. 2023, ApJL, 944, L15, doi: 10.3847/2041-8213/acac9e

Schruba, A., Leroy, A. K., Walter, F., et al. 2011, AJ, 142, 37, doi: 10.1088/0004-6256/142/2/37

Shetty, R., Glover, S. C., Dullemond, C. P., et al. 2011, MNRAS, 415, 3253, doi: 10.1111/j.1365-2966.2011.18937.x

Sorai, K., Kuno, N., Muraoka, K., et al. 2019, PASJ, 71, S14, doi: 10.1093/pasj/psz115

Sun, J., Leroy, A. K., Rosolowsky, E., et al. 2022, AJ, 164, 43, doi: 10.3847/1538-3881/ac74bd

Sun, J., Leroy, A. K., Ostriker, E. C., et al. 2023, ApJL, 945, L19, doi: 10.3847/2041-8213/acbd9c

Szűcs, L., Glover, S. C. O., & Klessen, R. S. 2014, MNRAS, 445, 4055, doi: 10.1093/mnras/stu2013

Teng, Y.-H., & Hirano, N. 2020, ApJ, 893, 63, doi: 10.3847/1538-4357/ab7cca

Teng, Y.-H., Sandstrom, K. M., Sun, J., et al. 2022, ApJ, 925, 72, doi: 10.3847/1538-4357/ac382f

Teng, Y.-H., Sandstrom, K. M., Sun, J., et al. 2023, ApJ, 950, 119, doi: 10.3847/1538-4357/accb86

Teng, Y.-H., Chiang, I.-D., Sandstrom, K. M., et al. 2024, ApJ, 961, 42, doi: 10.3847/1538-4357/ad10ae

Teng, Y.-H., Bolatto, A. D., Teuben, P. J., et al. 2026, ApJ, 1007, 59, doi: 10.3847/1538-4357/ae81b6

Villanueva, V., Bolatto, A. D., Vogel, S. N., et al. 2024, ApJ, 962, 88, doi: 10.3847/1538-4357/ad1387

Villanueva, V., Blaña, M., Bolatto, A. D., et al. 2025, A&A, 699, L11, doi: 10.1051/0004-6361/202555635

Virtanen, P., Gommers, R., Oliphant, T. E., et al. 2020, Nature Methods, 17, 261, doi: https://doi.org/10.1038/s41592-019-0686-2

Williams, T. G., Belfiore, F., Bureau, M., et al. 2025, MNRAS, 538, 3219, doi: 10.1093/mnras/staf498

Wright, E. L., Eisenhardt, P. R. M., Mainzer, A. K., et al. 2010, AJ, 140, 1868, doi: 10.1088/0004-6256/140/6/1868

Yajima, Y., Sorai, K., Miyamoto, Y., et al. 2021, PASJ, 73, 257, doi: 10.1093/pasj/psaa119